Squeezing Protein Shells: How Continuum Elastic Models, Molecular Dynamics Simulations, and Experiments Coalesce at the Nanoscale

W. H. Roos,[†‡] M. M. Gibbons,[§] A. Arkhipov,[¶‖] C. Uetrecht,[**††] N. R. Watts,[‡‡] P. T. Wingfield,[‡‡] A. C. Steven,[‡‡] A. J. R. Heck,[**††] K. Schulten,[¶‖] W. S. Klug,[§] and G. J. L. Wuite[†‡*]

[†]Natuur- en Sterrenkunde, [‡]Laser Centre, Vrije Universiteit, Amsterdam, The Netherlands; [§]Department of Mechanical and Aerospace Engineering, University of California, Los Angeles, California; [¶]Department of Physics, [‖]Beckman Institute, University of Illinois at Urbana-Champaign, Urbana, Illinois; **Biomolecular Mass Spectrometry and Proteomics Group, Utrecht Institute for Pharmaceutical Science and Bijvoet Center, Universiteit Utrecht, and [††]Netherlands Proteomics Centre, Utrecht, The Netherlands; and [‡‡]National Institute of Arthritis and Musculoskeletal and Skin Diseases, National Institutes of Health, Bethesda, Maryland

ABSTRACT The current rapid growth in the use of nanosized particles is fueled in part by our increased understanding of their physical properties and ability to manipulate them, which is essential for achieving optimal functionality. Here we report detailed quantitative measurements of the mechanical response of nanosized protein shells (viral capsids) to large-scale physical deformations and compare them with theoretical descriptions from continuum elastic modeling and molecular dynamics (MD). Specifically, we used nanoindentation by atomic force microscopy to investigate the complex elastic behavior of Hepatitis B virus capsids. These capsids are hollow, ~30 nm in diameter, and conform to icosahedral (5-3-2) symmetry. First we show that their indentation behavior, which is symmetry-axis-dependent, cannot be reproduced by a simple model based on Föppl-von Kármán thin-shell elasticity with the fivefold vertices acting as prestressed disclinations. However, we can properly describe the measured nonlinear elastic and orientation-dependent force response with a three-dimensional, topographically detailed, finite-element model. Next, we show that coarse-grained MD simulations also yield good agreement with our nanoindentation measurements, even without any fitting of force-field parameters in the MD model. This study demonstrates that the material properties of viral nanoparticles can be correctly described by both modeling approaches. At the same time, we show that even for large deformations, it suffices to approximate the mechanical behavior of nanosized viral shells with a continuum approach, and ignore specific molecular interactions. This experimental validation of continuum elastic theory provides an example of a situation in which rules of macroscopic physics can apply to nanoscale molecular assemblies.

INTRODUCTION

Nanoparticles are increasingly being used in a wide variety of applications in physics, chemistry, medicine, and materials science (1,2). For example, protein nanoshells are used in surface patterning or as nanocontainers and nanoreactors to encapsulate guest material for drug delivery and material synthesis (3,4). Despite their widespread applicability, however, a thorough understanding of their physical properties is still lacking, and it is increasingly being recognized that the ability to control such properties in an exact manner is essential for achieving optimal functionality (5). To fill this gap, we focused on the structure and mechanics of nanosized protein shells, i.e., icosahedral viral capsids. Empty viral shells (capsids) are valuable model systems for investigating the physical properties of nanosized objects because of the uniformity and high regularity of their structures. To date, most studies on the deformation of capsids have revealed a remarkably linear elastic force-indentation response that sometimes ends with abrupt failure of the shell (6–13). In the study presented here, we examine Hepatitis B virus (HBV) capsids, which reveal a different behavior, namely, a nonlinear but continuous response. HBV capsids exhibit two distinct icosahedral geometries (T=3 and T=4) that are self-assembled from 180 and 240 identical protein subunits, respectively. Because both capsid types are made up of the same building blocks, an a priori expectation is that any differences in mechanical response can be explained solely by their different geometries. We set out to quantitatively measure and model the mechanical response of these protein shells via a combination of atomic force microscopy (AFM), continuum elasticity theory and engineering structural analysis techniques (i.e., finite-element (FE) modeling), and coarse-grained (CG) molecular dynamics (MD). Focusing on the nonlinear and orientation-dependent indentation behavior, we sought to determine whether these CG modeling methods could adequately describe the mechanical response of these ~4 MDa nanocontainers over a large range of deformations.

MATERIALS AND METHODS

Atomic force microscopy

AFM experiments were conducted as described previously (14). Briefly, they consisted of experiments in liquid with a Nanotec Electronica (Madrid, Spain) atomic force microscope operated in jumping mode,

Submitted February 19, 2010, and accepted for publication May 20, 2010.

*Correspondence: gwuite@nat.vu.nl

M. M. Gibbons's present address is Department of Biomathematics, University of California, Los Angeles, California.

Editor: Gerhard Hummer.

0006-3495/10/08/1175/7 $2.00

doi: 10.1016/j.bpj.2010.05.033

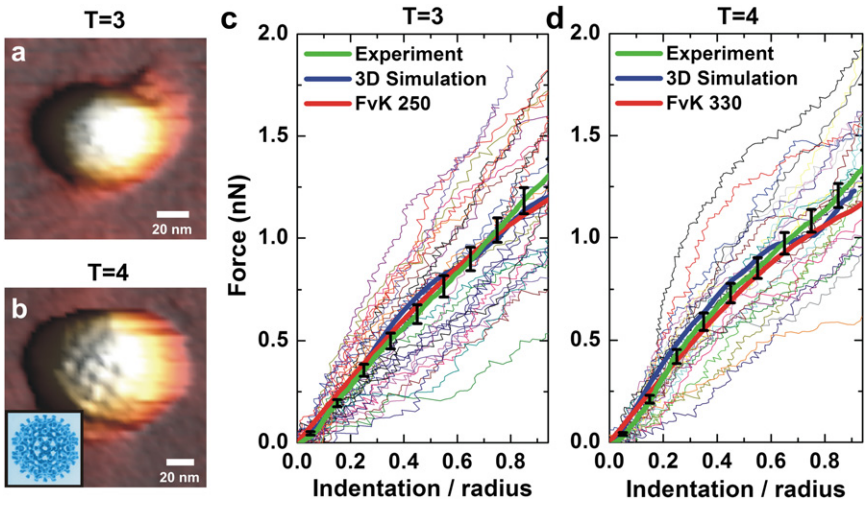

FIGURE 1 AFM images and FZ curves from experiment and FE models. (*a* and *b*) Whereas the AFM image of a T=3 particle (*a*) shows a relatively unstructured particle, that of a T=4 particle (*b*) shows substructures, presumably spikes (see Fig. S1 for a discussion about these spikes). The inset in *b* is a reconstruction of a T=4 particle, showing the spikes on its surface. (*c* and *d*) Individual experimental indentation curves on glass are printed as thin lines for the T=3 (*c*) and T=4 (*d*) particles. The average of these curves (Experiment) is plotted as a thick green line, with the error bars (SEM) in black. Also shown are the 3D FE simulation curves (*thick blue line*) and thin-shell curves (*thick red line*), which are both weighted averages of simulations along the two-, three-, and fivefold axes with respective weights of 30:20:12. The Supporting Material shows a zoom-in at the beginning of the curves (Fig. S2) and an analysis of the statistical relevance of the observed nonlinear effects (Fig. S3).

with 0.052 ± 0.002 N/m (± SD) rectangular OMCL-RC800PSA (Olympus) cantilevers. We attached cp149-3^{CA} HBV capsid mutants (14–16) to hydrophobic coverslips (6) by incubating a droplet of capsid solution (4.2 μM monomer concentration in 50 mM Tris, pH 7.5) for 20 min on a coverslip before starting the measurements. The presented data consist of the first AFM deformation curve (for each T=3 (n = 31, where n is the number of particles) and each T=4 (n = 25) particle) obtained using glass as the support material. Subsequent indentation curves were not used in the analysis presented here, because of effects of plasticity in the deformation. These effects are discussed in Arkhipov et al. (17). Test experiments on mica (n = 7) yielded similar nonlinear deformation curves. Errors are stated as the standard error of the mean (SEM) unless otherwise mentioned. All data were taken at a fixed loading rate (~1 nN/s). Order-of-magnitude changes in the loading rate are expected to elongate or contract the force scale at which the deformations occur by <10% (7). Because such changes are hard to distinguish within our scattered nonlinear curves, it is currently not feasible to check the loading rate dependence for this system.

Finite-element simulations

To create meshes for both the T=3 (data from a pseudo-atomic model) and T=4 (PDB-ID 1QGT) forms of the HBV capsid, we used the method described by Gibbons and Klug (18) for generating coarse three-dimensional (3D) tetrahedral FE meshes from x-ray crystal structures. The capsid deformation is modeled by finite-deformation continuum hyperelasticity, with a neo-Hookean constitutive law extended to the compressible regime (19,20). The strain energy density function is calculated as

$$W(\mathbf{C}) = \frac{\mu_0}{2}(I_1 - 3) + \frac{\lambda_0}{2}(\log J)^2 - \mu_0 \log J,$$

where I_1 = tr $\mathbf{C}$ and J = det $\mathbf{C}$ are invariants of the Right Cauchy-Green deformation tensor $\mathbf{C} = \mathbf{F}^T\mathbf{F}$, the metric associated with the gradient $\mathbf{F}$ of the deformation mapping, and λ_0 and μ_0 are the linearized Lamé constants, which can be related to the Young's modulus E and Poisson's ratio ν as $\lambda_0 = E\nu/[(1-2\nu)(1+\nu)]$ and $\mu_0 = E/2(1+\nu)$. The Cauchy stress is computed as $\boldsymbol{\sigma} = \mathbf{F}\mathbf{S}\mathbf{F}^T/J$ from the second Piola-Kirchhoff stress tensor $\mathbf{S} = 2\partial W/\partial \mathbf{C}$. The von Mises stress $\sqrt{3 s_{ij} s_{ij}/2}$ is a scalar invariant of the deviatoric part of the Cauchy stress $\mathbf{s} = \boldsymbol{\sigma} - (\text{tr}\,\boldsymbol{\sigma})\mathbf{I}/3$, commonly used in failure criteria for ductile materials.

Nanoindentation is simulated in a displacement-controlled fashion by vertically deforming the FE model between a flat substrate and a round AFM tip (R = 20 nm), both of which are modeled as rigid. Contact between the capsid and a rigid surface is modeled as rough, such that tangential slippage between contact surfaces is disallowed. The T=4 model has an average radius of 14.22 nm and an average shell thickness of 2.24 nm, comparable to the values reported by Wynne et al. (21). The T=3 model has an average radius of 12.40 nm and the same average thickness as the T=4 model.

Binning experimental FZ curves using FE simulations

By analyzing the 3D simulated curves for the three orientational axes (see Fig. 3) and their weighted average (Fig. 1, 3D simulation curves), we extract the following characteristics to bin the experimental curves in three orientational categories: 1), curves starting below the average are the twofold curves for T=3 and threefold curves for T=4; 2), the threefold curves for T=3 and twofold curves for T=4 start and end above the averaged curve; and 3), the fivefold curves of both morphologies start above the average and cross it at a relative indentation of ~0.7 and ~0.4 for T=3 and T=4, respectively. A similar comparison was performed for the thin-shell FE curves, such that all curves below the average were assigned to the fivefold axis for both T=3 and T=4 particles. The two- and threefold curves are binned together because of their similar indentation behavior.

Thin-shell simulations

The thin-shell simulations model the capsid as an icosahedral shell surface with elastic energy described by Föppl-von Kármán (FvK) thin-shell elasticity as

$$F = \int \left[\frac{\kappa}{2}(2H)^2 + \frac{\lambda}{2}(E_{ii})^2 + \mu\left(E_{ij}E_{ij}\right)\right] dA,$$

where κ is the bending modulus as described above, and λ and μ are the 2D Lamé constants (22). As described by Klug et al. (8), the stress-free reference shell surface is discretized with triangular subdivision-surface FEs and

the energy is relaxed by numerical optimization using the Broyden-Fletcher-Goldfarb-Shanno (BFGS) method (23) to determine a prestressed equilibrium shape, which is then subjected to displacement-controlled indentation between a rigid plate and a rigid hemispherical AFM-tip surface of radius equal to the average capsid radius. Contacts between the capsid and rigid surfaces are modeled as rough, just as in the 3D simulations. Mesh refinement studies showed that a mesh of 2562 nodes and 5120 elements gave reasonably converged, mesh-independent results. Using Eq. 1 and inserting the averaged particle radius as extracted from the crystal structures, we determine an effective mechanical thickness of 2.48 nm for both the T=3 and the T=4 particles of the FvK simulations. This value, which is comparable to that obtained from the crystal-structure geometry, represents the effective thickness of a uniform icosahedral shell having the same mechanical stiffness as the nonuniform shell used in experiments.

Molecular dynamics simulations

The MD simulations were performed as described previously (17). In brief, they consisted of a shape-based CG (SBCG) model (24) employing 15 CG beads to represent each monomer of the T=4 HBV capsid (i.e., ~150 atoms per bead), distributed according to the protein shape (PDB ID: 1QGT) (21) by a topology-representing map algorithm (24,25). One SBCG monomer is replicated to construct the full capsid (240 monomers). Within the monomer, the total mass and charge of the atoms constituting the Voronoi cell of each bead are assigned to that bead, and two beads are connected by a bond if the two Voronoi cells are connected by the protein backbone. The T=4 capsid consists of dimers formed by closely associated monomers (21) (in the SBCG model, such monomers are connected by three bonds; beyond that, no intermonomer bonds are established). The solvent is treated implicitly as a viscous medium (24). The substrate and AFM tip are modeled as cubic lattices of CG beads (with a period of 1.5 nm). The substrate is a single sheet of such a lattice, and the tip is carved out of the lattice into a hemisphere with a 15 nm radius. The SBCG beads interact with each other through Lennard-Jones (LJ) and Coulomb potentials, and harmonic potentials are introduced for all bonds, as well as for angles formed by triples of bonded beads. The bonded potentials (bonds and angles) are parameterized to reproduce the protein stiffness observed in an all-atom simulation of a monomer. The nonbonded potential (LJ and Coulomb) is tuned so that the SBCG capsid simulated without the AFM tip and substrate will maintain its correct spherical shape, diameter, and thickness (21). Of interest, CGMD simulations suggest that native contacts between monomers remain preserved in the T=4 capsid even in the case of very strong deformation: the number of native contacts remains in the range of 75–89% in the cases of both reversible indentation of 0.35R and irreversible indentation as deep as 1.25 R (as reported previously (17)). Thus, appropriate modeling of interactions in the native structure of the T=4 HBV capsid is essential for capturing the deformation dynamics. The dynamics of the SBCG system is described by the Langevin equation (24), with a damping constant of 2 ps^{-1}. Simulations are done at a temperature of 300 K and an integration time step of 150 fs. The AFM tip is moved in the z-dimension at a velocity of 2.3 nm/μs using steered MD (26). SBCG MD simulations cover 5–10 μs for one indentation round, depending on the chosen indentation depth and relaxation time for the capsid after the AFM tip is retracted. The simulations were performed with NAMD (27) and the molecular graphics (see Fig. 5) were generated using VMD (28).

RESULTS AND DISCUSSION

Using AFM, we first image and subsequently indent the HBV shells while recording the force-distance (FZ) curves (6,11,29,30) (Fig. 1). When we indent the particles with forces below 0.8 nN, both the T=3 and T=4 capsids behave reversibly upon indentation, and no material fatigue occurs after multiple indentations at these small forces (14). Indentation experiments at significantly higher forces (~2 nN) result in a continuous indentation response that exhibits subtle but noticeable nonlinearities (Fig. 1, *c* and *d*), with similar results obtained on glass and mica. The robustness of the nonlinear response was tested statistically as shown in Fig. S3 of the Supporting Material. As the nonlinear behavior is seen at rather large indentations (approximately one-half the capsid radius), it cannot be attributed to the small-strain, Hertz-like stiffening stemming from increasing contact area with the tip (29,31). Rather, nonlinear softening is consistent with the geometry of thinner spherical shells, signifying a transition of the load-bearing mechanism from in-plane stretching to transverse bending (31).

As can be seen in Fig. 1, there is substantial variation between the individual FZ curves. In one other recent study on a different icosahedral virus (minute virus of mice (MVM)), variation in the linear capsid mechanical response was linked to anisotropy in genome packaging (30). However, whereas for MVM no orientation-dependent indentation behavior was observed for the empty capsids, here we consider the hypothesis that the spread of FZ curves reflects the different orientations in which empty HBV capsids are affixed to the substrate. Because the diameters of an HBV capsid along the two-, three-, and fivefold symmetry axes are nearly identical, assignment of a given indentation curve to a particular symmetry axis cannot be done on the basis of height data alone. Furthermore, no orientation-specific features could be imaged on the capsid surface. This ambiguity prompts the question as to whether capsid orientations can be distinguished by other means. In particular, recent modeling studies of the indentation of the cowpea chlorotic mottle virus (CCMV) predict that the mechanical response may show orientation dependence at large indentations where nonlinear effects are pronounced (18). Here, nonlinearities in the experimental response of HBV capsids provide an opportunity to address the suitability of indentation response as a reporter for capsid orientation, as well as a means to test the predictive validity of the continuum elasticity models.

Following our hypothesis regarding the orientation-dependent indentation behavior of HBV shells, we performed simulations using 3D topographically detailed, FE models derived from crystal structures using the methodology described by Gibbons and Klug (18). Indentation was simulated on capsid models in three distinct orientations, with the indentation axis aligned with the two-, three-, and fivefold symmetry axes (Fig. 2). These models incorporate a simple homogeneous, isotropic, nonlinear elastic stress-strain response that scales in proportion to the initial Young's modulus. To obtain the correct Young's modulus, we first average the simulated indentation curves along the different symmetry axis with the correct weighting for the relative occurrence of the symmetry axis (30:20:12 for the two-, three-, and fivefold axes, respectively) and compare this curve with the averaged experimental curves (Fig. 1, 3D

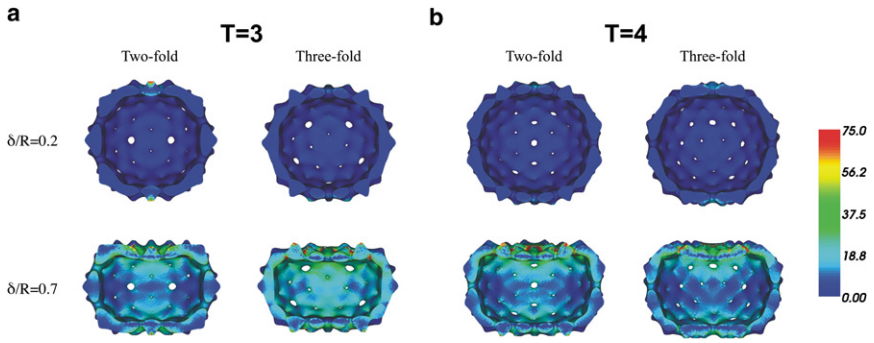

FIGURE 2 Snapshots of 3D FE meshes. Indentation of T=3 (*a*) and T=4 (*b*) HBV capsids along their two- and threefold symmetry axes. Capsid shapes for two different relative deformations (indentation/radius, δ/R) are shown. Whereas for small deformations the von Mises stresses (depicted in MPa) are mainly apparent at the contact points with the tip and the surface (*top* and *bottom*), for large deformations they are significant in considerable parts of the deformed shells. In particular, at larger deformations, as shown in the lower panels, the stresses are maximized at the inner and outer surfaces of the capsid wall with smaller values in the interior, consistent with bending as the primary load transfer mechanism.

simulation). The *y*-axis scaling of these simulated indentations yields a Young's modulus $E = 0.26$ GPa for both shells (T=3 and T=4). Similar Young's moduli were expected because both particle morphologies are constructed from the same protein building blocks.

Next, having determined the Young's modulus of the system, we can compare the orientation-dependent FZ response obtained for the 3D FE model with the experimental results. Fig. 3 shows a large variation in FZ response when the virus is indented along different axes. Guided by the characteristic shapes of the different model curves, we can now bin (see Materials and Methods) the experimental FZ curves into three orientations (Fig. 4). Because the relative occurrence of the various symmetry sites is known, when the icosahedral capsids attach randomly to the substrate, the expected frequency of FZ curves will be highest for the predicted twofold symmetry axis force response, intermediate for the threefold force response, and lowest for the fivefold response. A distribution that matches the different occurrences of these symmetry axes is indeed what we observe for both the T=3 and T=4 shells using the model-based binning procedure (Table S1). After separating the individual FZ curves in the different orientations, we observe a relatively small spread for each category (Fig. 4). This result indicates that the large spread of the experimental data, as seen in Fig. 1, indeed seems to originate from the symmetry axis-dependent indentation behavior of the particles.

Although nonlinearities in the indentation response of the 3D model are chiefly caused by variations in shell thickness and contact geometry of the tip with the topographically nonuniform shell, these features are not the only potential sources for orientation-dependent mechanics. Recent FvK thin-shell elasticity studies that modeled capsids as icosahedral shells containing prestressed disclinations at the fivefold icosahedral vertices (8,22,32–34) also showed orientation dependence in the indentation response. Here, we evaluate the usefulness of this description for interpreting the nonlinear deformation behavior of HBV capsids. In thin-shell theory, local stretching of the surface induces strain energy scaled by the 2D Young's modulus $Y = Et$, with t denoting the shell thickness. The energy of out-of-plane

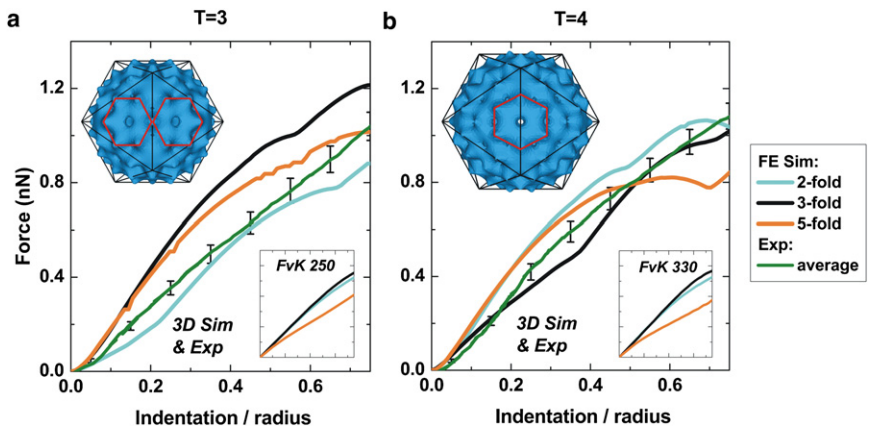

FIGURE 3 Separation along symmetry axes for the T=3 (*a*) and T=4 (*b*) morphologies. The main graphs show the 3D FE simulation and the averaged experimental results. The threefold orientation of the T=3 particles and the twofold orientation of the T=4 particles show the stiffest curves. Of interest, both these orientations coincide with the quasi-sixfold symmetry axis, resulting in the highest contact area. For the T=4 conformation at large indentations, the force curves for both the two- and fivefold orientations noticeably soften as a result of the transition from stretch-bending to pure bending. This transition is amplified due to the ease of bending the thinner areas of the capsid, which occur in a circular ring around the contact area. This effect has been observed in CCMV as well (18). The upper-left insets show the respective HBV capsid models viewed along their twofold symmetry axis. The capsids are depicted inside an icosahedral cage (*black*) and with quasi-sixfold symmetry shown as red hexagons. The lower-right insets show the respective thin-shell FE simulation results, where the axes are identical to those of the main graphs.

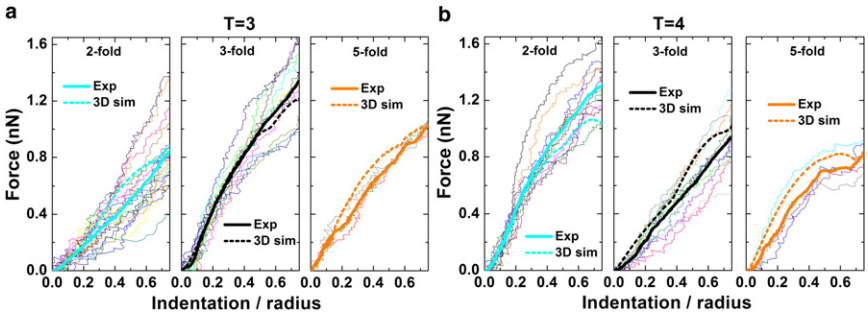

FIGURE 4 Experimental curves grouped by apparent orientation. Individual experimental curves are grouped according to the binning procedure based on the curves obtained from the 3D FE model (see Fig. 3 and main text). The experimental curves for the T=3 (*a*) and T=4 (*b*) capsids are plotted together with the corresponding model. The grouping results in a reduced spread of the experimental indentation curves, and inferred orientation statistics that are consistent with the hypothesis of orientation-dependent indentation behavior.

bending of the surface is scaled by a flexural rigidity κ, which is classically given as $\kappa = Et^3/[12(1-\nu^2)]$, with ν denoting Poisson's ratio, for which a value of 0.4 is used here (31). The FvK number $\gamma = YR^2/\kappa$, with the particle radius R, is a dimensionless parameter that emerges naturally as a measure of the ratio of the in-plane elasticity of the shell to its out-of-plane bending rigidity. Considering a thin-shell model as approximating a homogeneous 3D shell, the FvK number can then be expressed as

$$\gamma = 12\left(1-\nu^2\right)\left(\frac{R}{t}\right)^2. \quad (1)$$

Numerical simulations based on thin-shell elasticity reveal a strong variation of the force-indentation response with FvK number (8). Simulations of capsids with $\gamma \lesssim 150$ show a linear response (Fig. S4) (8). For large γ ($\gtrsim 800$) the FZ curves are roughly linear up to an indentation of ~0.4 times the radius, at which point the shell buckles, as indicated by a precipitous drop in force. In the intermediate range ($150 \lesssim$ FvK $\lesssim 800$), the response becomes increasingly nonlinear but does not involve buckling. The theoretical FvK values for the two HBV shells are ~250 for T=3 and ~400 for T=4 using Eq. 1 and reported dimensions (14,15). To verify the predicted existence of a continuous nonlinear elastic response for HBV shells, we simulated FZ curves for a range of FvK values. The best fits to the experimental data were obtained with FvK values of 250 and 330 for T=3 and T=4, respectively, close to the theoretical values (Fig. 1). Despite the good match among the orientation-averaged thin-shell curves, a detailed examination of the curves for individual symmetry axes shows that the uniform thin-shell theory (Fig. 3, *insets*) and the nonuniform 3D models make different predictions of orientation dependence (Fig. 3). Specifically, the thin-shell theory predicts that the response along the fivefold axis will always be softer than that along the other axes, whereas the 3D models predict that the twofold (T=3) and threefold (T=4) axes will have the softest response. However, attempts to bin the experimental data using the thin-shell simulation results produced a ratio of the number of capsids lying on the various symmetry sites that is inconsistent with the frequency of these sites occurring on an individual capsid (Table S1). This suggests that prestress at the fivefold icosahedral vertices of the capsid, predicted by thin-shell disclination models (8,22,32–34), is, for HBV, not the dominant mechanism in determining the orientation dependence of the mechanical response.

The success of detailed FE modeling in quantitatively recapitulating the measured deformation of these nanosized objects prompted us to ask whether similar results could be obtained by starting the simulations from atomic interactions. Hence, we set out to apply a SBCG MD model (24) to capture the indentation behavior of the T=4 HBV capsids as previously described (17). A previous MD simulation of

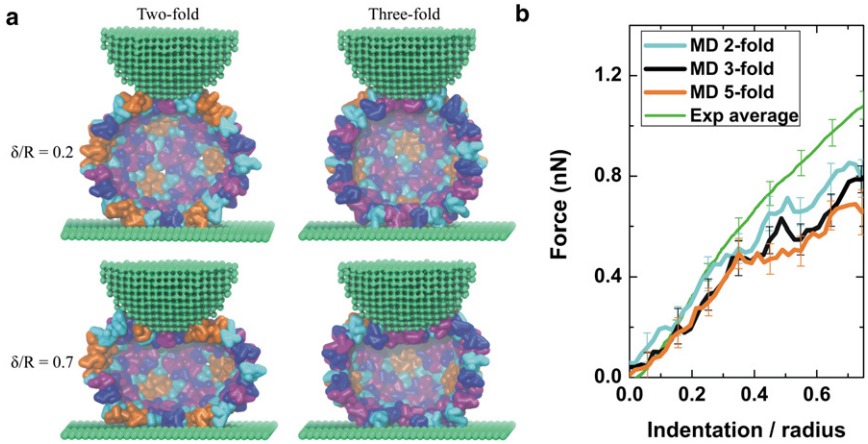

FIGURE 5 SBCG MD simulation results. (*a*) SBCG MD representation of an AFM tip indenting a T=4 HBV capsid at the same relative indentations and along the same pushing directions as those shown in Fig. 2 *b* for the FE model. Capsid protein monomers are shown in alternating colors. (*b*) MD indentation curves (averaged over time windows of 150 ns and all simulations, $n = 5$) along the two-, three-, and fivefold symmetry axes, and average of all experimental indentation curves. The experimental indentation curves are divided by their measured radius and then averaged. The averaged MD curves are divided by the outer radius used for the simulations.

a viral shell captured deformation on a nanosecond timescale using a nonrealistically small indenter (35). In our MD simulation (accounting for solvent through a Langevin approach), we obtained the deformation behavior of a capsid on a microsecond timescale using a tip similar in size to a regular AFM tip (Fig. 5 *a*). Note that another recent study (36) reported CG simulations of nanoindentations of CCMV and CPMV capsids, and demonstrated an agreement between these simulations and the continuum elastic model in terms of the force response.

Deformation of the capsid in SBCG MD simulations is illustrated in Fig. 5 *a* by snapshots from two representative trajectories. The deformation is similar to that observed in the FE simulations (Fig. 2 *b*). It is important to note that individual SBCG MD simulations follow different trajectories, whereas FE simulations provide an average description of the indentation. Several SBCG MD trajectories were obtained for each pushing direction, and whereas the dynamics of the capsid differ slightly from one trajectory to the other, overall the observed deformations are approximately the same for all trajectories that employ the same pushing direction (see details in Arkhipov et al. (17)). The unscaled MD indentation curves along the three major symmetry axes in Fig. 5 *b* reveal a good fit to experimental data, especially at the beginning of the indentation curves. Because the MD model is tuned simply to reproduce a stable undeformed capsid of the correct dimensions, the best fit is also expected for small deformations. Next, the symmetry axis-dependent deformations seen in these simulations show that capsids are stiffest near the twofold axes, and that deformations near the fivefold axes plateau around a relative indentation of ~0.4. These observations are in line with the detailed FE predictions (Fig. 3 *b*) and the experimental results (Fig. 4 *b*).

CONCLUSIONS

The observed agreement between the CG MD curves and the experimental data is especially satisfying considering that the MD model was parameterized without any knowledge of its deformation or interaction with the AFM tip or substrate. Hence, whereas the FE results need to be scaled to fit the experiments, the MD simulations can reproduce the experimental results without using experimental indentation data to tune parameters or perform scaling. This outcome suggests that even when few experimental data are available, CG MD simulations can be used to provide an estimate of the material properties of nanostructures.

To conclude, the indentation responses of HBV along individual symmetry axes seem to be more accurately represented by the 3D FE model than by the thin-shell model. We show that this observation can be exploited by using predicted 3D FE modeling curves to assign the experimental data into separate data sets, each reflecting indentations along different symmetry axes. In addition, we show that CG MD simulations based on atomic interactions within the 4 MDa viral nanostructure can also faithfully describe the elastic nonlinear response of a viral nanoshell to compressive deformation. However, the success of the 3D models in simulating the more detailed response for large indentations indicates to us that the nonuniform surface topography included in those models can have tangible effects on the force-indentation profile, to a degree that increases as indentation proceeds. Thus, continuum models can describe not only quantitatively linear features, but also key nonlinear features. These results support the idea that the length scale over which heterogeneous atomic/molecular interactions average out to a more homogeneous continuum-like elastic behavior is rather small, perhaps comparable to the size of the individual proteins.

SUPPORTING MATERIAL

Four figures and a table are available at http://www.biophysj.org/biophysj/supplemental/S0006-3495(10)00672-7.

This work was supported by a NanoSci-E+ grant administered by Stichting voor de Technische Wetenschappen (G.J.L.W.), the Netherlands Organisation for Scientific Research through a CW-ECHO grant (G.J.L.W.), a Rubicon grant (W.H.R.), a CAREER Award from the National Science Foundation (CMMI-0748034 to W.S.K.), grants DMS-0349195 (M.M.G.) and PHY0822613 (K.S.), supercomputer time (MCA93S028), National Institutes of Health grants K25AI058672 and 5T32AI060567-05 (M.M.G.) and P41-RR005969 (K.S.), and the intramural research program of the National Institute of Arthritis and Musculoskeletal and Skin Diseases (N.R.W., P.T.W., and A.C.S.). M.M.G. was supported by a Graduate Assistance in Areas of National Need fellowship from the U.S. Department of Education, and A.A. was supported by an L. S. Edelheit fellowship.

REFERENCES

1. Fischlechner, M., and E. Donath. 2007. Viruses as building blocks for materials and devices. *Angew. Chem. Int. Ed. Engl.* 46:3184–3193.
2. Peer, D., J. M. Karp, …, R. Langer. 2007. Nanocarriers as an emerging platform for cancer therapy. *Nat. Nanotechnol.* 2:751–760.
3. Douglas, T., and M. Young. 1998. Host-guest encapsulation of materials by assembled virus protein cages. *Nature.* 393:152–155.
4. Smith, J. C., K. B. Lee, …, C. A. Mirkin. 2003. Nanopatterning the chemospecific immobilization of cowpea mosaic virus capsid. *Nano Lett.* 3:883–886.
5. Mitragotri, S., and J. Lahann. 2009. Physical approaches to biomaterial design. *Nat. Mater.* 8:15–23.
6. Ivanovska, I. L., P. J. de Pablo, …, G. J. Wuite. 2004. Bacteriophage capsids: tough nanoshells with complex elastic properties. *Proc. Natl. Acad. Sci. USA.* 101:7600–7605.
7. Michel, J. P., I. L. Ivanovska, …, C. F. Schmidt. 2006. Nanoindentation studies of full and empty viral capsids and the effects of capsid protein mutations on elasticity and strength. *Proc. Natl. Acad. Sci. USA.* 103:6184–6189.
8. Klug, W. S., R. F. Bruinsma, …, G. J. Wuite. 2006. Failure of viral shells. *Phys. Rev. Lett.* 97:228101.
9. Ivanovska, I., G. Wuite, …, A. Evilevitch. 2007. Internal DNA pressure modifies stability of WT phage. *Proc. Natl. Acad. Sci. USA.* 104: 9603–9608.

10. Gibbons, M. M., and W. S. Klug. 2007. Mechanical modeling of viral capsids. *J. Mater. Sci.* 42:8995–9004.

11. Roos, W. H., and G. J. L. Wuite. 2009. Nanoindentation studies reveal material properties of viruses. *Adv. Mater.* 21:1187–1192.

12. Liashkovich, I., W. Hafezi, …, V. Shahin. 2008. Exceptional mechanical and structural stability of HSV-1 unveiled with fluid atomic force microscopy. *J. Cell Sci.* 121:2287–2292.

13. Roos, W. H., K. Radtke, …, G. J. Wuite. 2009. Scaffold expulsion and genome packaging trigger stabilization of herpes simplex virus capsids. *Proc. Natl. Acad. Sci. USA.* 106:9673–9678.

14. Uetrecht, C., C. Versluis, …, A. J. Heck. 2008. High-resolution mass spectrometry of viral assemblies: molecular composition and stability of dimorphic hepatitis B virus capsids. *Proc. Natl. Acad. Sci. USA.* 105:9216–9220.

15. Zlotnick, A., N. Cheng, …, P. T. Wingfield. 1996. Dimorphism of hepatitis B virus capsids is strongly influenced by the C-terminus of the capsid protein. *Biochemistry.* 35:7412–7421.

16. Wingfield, P. T., S. J. Stahl, …, A. C. Steven. 1995. Hepatitis core antigen produced in *Escherichia coli*: subunit composition, conformational analysis, and in vitro capsid assembly. *Biochemistry.* 34: 4919–4932.

17. Arkhipov, A., W. H. Roos, …, K. Schulten. 2009. Elucidating the mechanism behind irreversible deformation of viral capsids. *Biophys. J.* 97:2061–2069.

18. Gibbons, M. M., and W. S. Klug. 2008. Influence of nonuniform geometry on nanoindentation of viral capsids. *Biophys. J.* 95:3640–3649.

19. Holzapfel, G. A. 2001. Nonlinear Solid Mechanics: A Continuum Approach for Engineering. Wiley, New York.

20. Gurtin, M. E. 1981. An Introduction to Continuum Mechanics. Academic Press, New York.

21. Wynne, S. A., R. A. Crowther, and A. G. W. Leslie. 1999. The crystal structure of the human hepatitis B virus capsid. *Mol. Cell.* 3:771–780.

22. Lidmar, J., L. Mirny, and D. R. Nelson. 2003. Virus shapes and buckling transitions in spherical shells. *Phys. Rev. E.* 68:051910.

23. Zhu, C. Y., R. H. Byrd, …, J. Nocedal. 1997. Algorithm 778: L-BFGS-B: Fortran subroutines for large-scale bound-constrained optimization. *ACM Trans. Math. Softw.* 23:550–560.

24. Arkhipov, A., P. L. Freddolino, and K. Schulten. 2006. Stability and dynamics of virus capsids described by coarse-grained modeling. *Structure.* 14:1767–1777.

25. Martinetz, T., and K. Schulten. 1994. Topology representing networks. *Neural Netw.* 7:507–522.

26. Sotomayor, M., and K. Schulten. 2007. Single-molecule experiments in vitro and in silico. *Science.* 316:1144–1148.

27. Phillips, J. C., R. Braun, …, K. Schulten. 2005. Scalable molecular dynamics with NAMD. *J. Comput. Chem.* 26:1781–1802.

28. Humphrey, W., A. Dalke, and K. Schulten. 1996. VMD: visual molecular dynamics. *J. Mol. Graph.* 14:33–38, 27–28.

29. Kol, N., M. Gladnikoff, …, I. Rousso. 2006. Mechanical properties of murine leukemia virus particles: effect of maturation. *Biophys. J.* 91:767–774.

30. Carrasco, C., M. Castellanos, …, M. G. Mateu. 2008. Manipulation of the mechanical properties of a virus by protein engineering. *Proc. Natl. Acad. Sci. USA.* 105:4150–4155.

31. Gibbons, M. M., and W. S. Klug. 2007. Nonlinear finite-element analysis of nanoindentation of viral capsids. *Phys. Rev. E.* 75:031901.

32. Nguyen, T. T., R. F. Bruinsma, and W. M. Gelbart. 2005. Elasticity theory and shape transitions of viral shells. *Phys. Rev. E.* 72:051923.

33. Vliegenthart, G. A., and G. Gompper. 2006. Mechanical deformation of spherical viruses with icosahedral symmetry. *Biophys. J.* 91:834–841.

34. Buenemann, M., and P. Lenz. 2007. Mechanical limits of viral capsids. *Proc. Natl. Acad. Sci. USA.* 104:9925–9930.

35. Zink, M., and H. Grubmüller. 2009. Mechanical properties of the icosahedral shell of southern bean mosaic virus: a molecular dynamics study. *Biophys. J.* 96:1350–1363.

36. Cieplak, M., and M. O. Robbins. 2010. Nanoindentation of virus capsids in a molecular model. *J. Chem. Phys.* 132:015101.